Film Straining of Colloids in Unsaturated Porous Media: Conceptual Model and Experimental Testing

ARTICLE *in* ENVIRONMENTAL SCIENCE AND TECHNOLOGY · JULY 1997

Impact Factor: 5.33 · DOI: 10.1021/es970017q

2 AUTHORS:

Jiamin Wan
Lawrence Berkeley National Laboratory
126 PUBLICATIONS **2,658** CITATIONS
SEE PROFILE

Tetsu K. Tokunaga
Lawrence Berkeley National Laboratory
156 PUBLICATIONS **2,937** CITATIONS
SEE PROFILE

Environ. Sci. Technol. **1997**, *31*, 2413−2420

Film Straining of Colloids in Unsaturated Porous Media: Conceptual Model and Experimental Testing

JIAMIN WAN* AND TETSU K. TOKUNAGA

Earth Sciences Division, Lawrence Berkeley National Laboratory, Berkeley, California 94720

A film-straining theory is introduced, which proposes that transport of suspended colloids can be retarded due to physical restrictions imposed by thin water films in partially saturated porous media. A quantitative, mechanistic model is provided to predict the film-straining efficiency. In this model, the concepts of "critical matric potential" and "critical saturation" are introduced, at which thick film interconnections between pendular rings are broken and film straining begins to become effective. The modeled magnitude of colloid transport through water films depends on the ratio of colloid size to film thickness and on flow velocity. Effective penetration of hydrophilic colloids through unsaturated porous media is predicted when a system is above the critical saturation value. For colloids smaller than the thickness of adsorbed thin water films, the model predicts that colloids can still be efficiently transported, even when the system matric potential and saturation are lower than their critical values. The model was tested through experiments on transport of hydrophilic latex particles (four sizes from 0.01 to 1.0 μm) in sand columns of three different grain sizes and at flow rates spanning 4 orders of magnitude. The conceptual basis of this model is supported by good agreement between the wide range of experiments and model predictions using only two adjustable parameters.

Introduction

Transport of colloids in subsurface environments has received considerable attention in recent years, primarily because suspended colloids (inorganic, organic, and microbial) can be contaminants themselves and can serve as carriers of sorbed contaminants (*1*, *2*). Current conceptual and predictive models for colloid transport in soils and groundwaters have relied heavily on filtration theory, developed for single fluid phase systems (*3*−*5*). In filtration theory, two general categories of colloid removal are most relevant to groundwater systems: straining and physical−chemical surface deposition. Straining occurs in small pore restrictions and is considered to become important when the ratio of colloid size (d) to the porous medium's characteristic grain size (D) exceeds a certain range. The critical d/D is typically in the range of 0.05−0.2 (*5*, *6*). In this paper, we refer to the straining mechanism in filtration theory as "conventional straining". Physical−chemical deposition processes involve two steps, collision (interception, diffusion, sedimentation) and attachment (electrostatic forces, van der Waals forces, hydrophobic forces), resulting in colloid deposition onto grain surfaces. Filtration theory has been well developed over the past few decades. However, filtration theory does not account for the effect of unsaturation.

Colloid transport through the unsaturated zone has many important environmental consequences. Vadose environments are typically rich in mineral, organic, and microbial colloids, and contaminant sources are usually located in the vadose zone, closed to ground surface. Contaminant-bearing colloids may move downwards through the vadose zone and into groundwater. Although the majority of research on colloid transport has been conducted on water-saturated porous media (*7*−*12*), interest in unsaturated colloid transport has rapidly increased in the recent years (*13*−*19*). Many experiments on unsaturated transport of colloids, including bacteria and viruses, have demonstrated the general trend that colloid retention is more efficient when a soil is drier than when it is wetter. Wan and Wilson (*16*, *17*) and Wan et al. (*18*) introduced the mechanism of attachment of colloids and bacteria at gas−water interfaces in porous media. This mechanism has become accepted as a factor controlling the fate and transport of colloidal particles in the vadose zone. However, uniformity of water saturations was probably not achieved along some of the columns used in these previous studies (*17*, *18*). The upper ends of the less saturated columns were probably considerably drier than the bottom ends. In view of the theory and experiments we present in this paper, it is quite likely that some of the results from the previous studies reflect the influences of both attachment at gas−water interfaces and retardation within thin films. In considering the past work as well as this present one, it is worth noting that a comprehensive theory for unsaturated colloid filtration has yet to be developed.

In this paper, we propose that the gas phase can physically constrain colloid movement through regions of thin water films. The mechanistic basis of this process, which we call "film straining" is developed, followed by predictions of its macroscopic consequences and comparisons with a series of unsaturated colloid transport experiments.

Conceptual Model

In partially saturated porous media, water is retained by capillarity and adsorption, with both effects included in the matric potential, ψ (energy per unit volume, Pa). The matric potential represents the saturation-dependent component of the chemical potential of water (*20*, *21*). Figure 1A,B illustrates water retained by capillarity as pendular rings around grain−grain contacts and retained by adsorption as thin films along grain surfaces. The pendular rings in Figure 1A,B exhibit two different states of connectivity. The pendular rings in Figure 1A show the critical condition at which pendular rings are on the verge of disconnecting. We define the saturation at which pendular rings become discontinuous as the critical saturation, S_c, and its corresponding matric potential at this point as critical matric potential, ψ_c. We propose that film straining occurs only when pendular rings become disconnected. This condition of complete pendular ring disconnection is shown in Figure 1B. In this state, colloids must move through adsorbed thin water films in their traverse through the porous medium. Figure 2 is a closeup look of one point on the adsorbed film region in Figure 1B. We propose that when the thickness of an adsorbed water film, w, is greater than the diameter of a spherical colloid particle, d, film straining of hydrophilic colloids remains ineffective, even below S_c (Figure 2A). However, when w is similar or smaller than d, retardation of colloid transport is expected since surface tension forces hydrophilic colloids against grain

* Corresponding author phone: 510-486-6004; fax: 510-486-7797; e-mail: jwan@lbl.gov.

S0013-936X(97)00017-5 CCC: $14.00

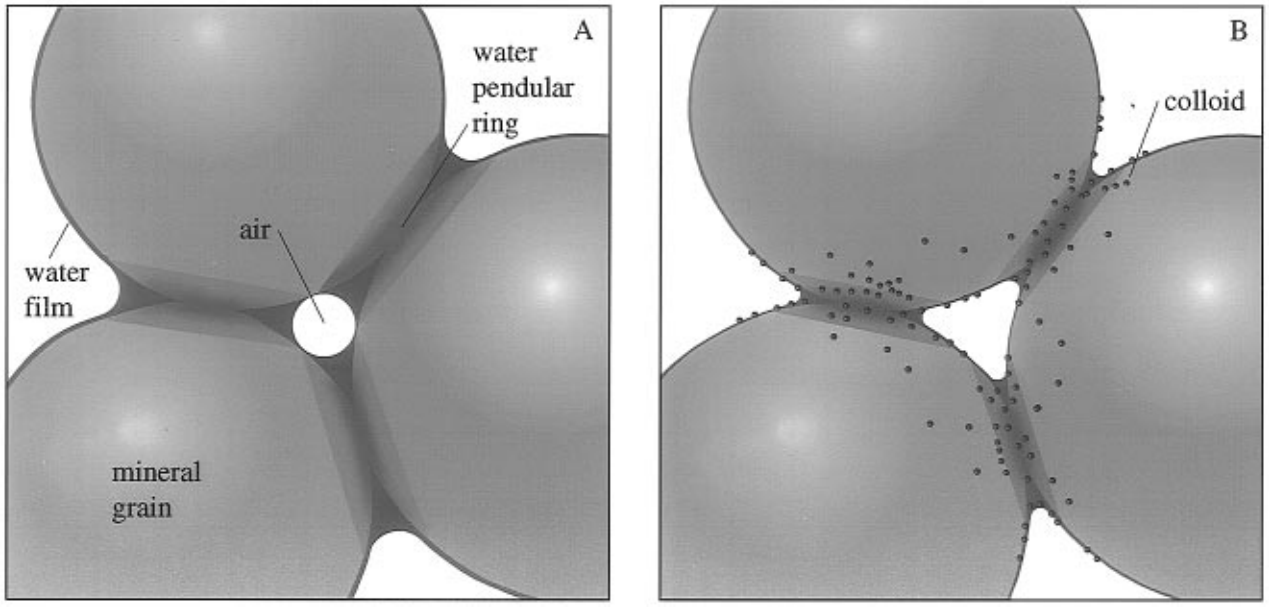

FIGURE 1. Conceptual model of unsaturated straining. (A) Pendular rings are at the verge of disconnecting. (B) Pendular rings are disconnected (connected only by thin films). Colloids are retained within the pendular rings and in water films.

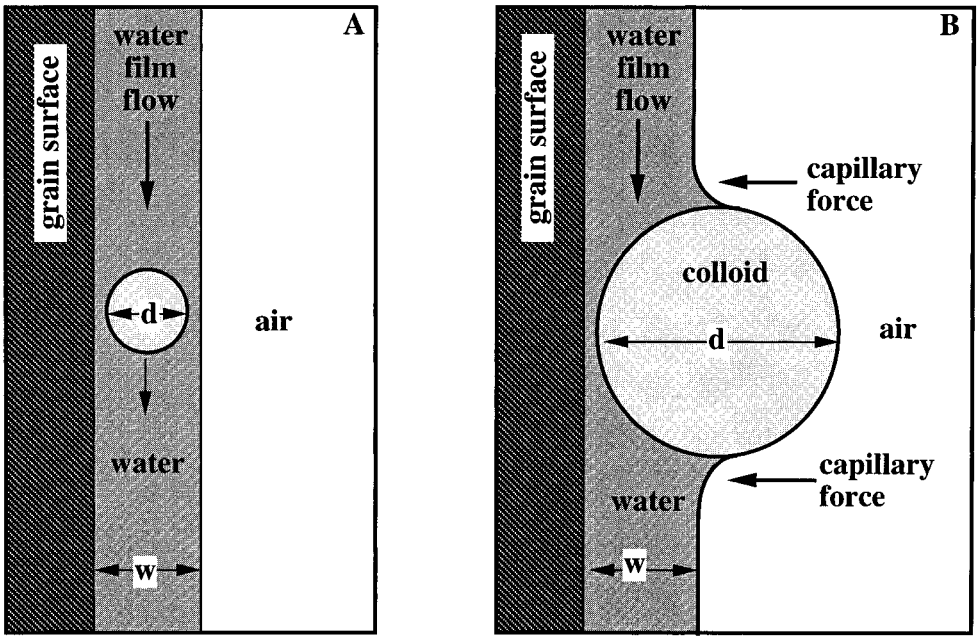

FIGURE 2. Conceptual model of a closeup view of the thin water film region in Figure 1B. When *dlw* < 1(A), film straining is inefficient, but when *dlw* > 1 (B) film straining occurs.

surfaces (Figure 2B). Therefore, pendular ring discontinuity and the ratio of colloid size to film thickness are clearly important factors controlling unsaturated colloid transport. Retardation of ideal, nonsorbing colloids can occur at two locations: trapped within individual pendular rings due to exclusion from entry into surrounding thin films and within films that are too thin to effectively move the colloids. In this model, we are not concerned with colloid retardation caused by other mechanisms, conventional straining, physical–chemical deposition, and sorption at the gas–water interfaces, since these already recognized processes can be included latter. While the local S_c for pendular ring merging is a unique value for given local configuration of grains, hysteresis in the moisture characteristic (the relation between S and ψ) prevents identification of a generally unique local ψ_c. However, since the matric potential is more directly related to film thickness, it will be used in the following development, and unique values of the matric potential will be considered in the conceptual model through referencing the main wetting curve.

In order to develop a predictive model for unsaturated straining of colloids, we begin by considering a system with simple geometry. We consider a close-packing (rhombohedral packing) of uniform spherical grains of radius R and menisci forming pendular rings around grain contacts. Figure 1A depicts a coplanar cross-section through three neighboring grains, with their pendular rings barely touching, i.e., at S_c. This illustration indicates that a unique local S_c can be defined for a particular grain packing, regardless of scale. In other words, a common value of S_c exists for geometrically similar media (*22*). However, scale (grain size) remains important in determining ψ_c as the Laplace–Young equation shows

$$\psi_c = \frac{-B\gamma}{R} \qquad (1)$$

where B is a constant characteristic of the packing geometry and grain surface wettability (*23*, *24*), and γ is the water−gas surface tension. In the case of a close packing of perfectly water-wettable (zero contact angle) spherical grains illustrated in Figure 1B, we have $\psi_c = -9.068\gamma/D$. At $\psi > \psi_c$, and $S > S_c$, i.e., at energies and saturations higher than their critical values, unsaturated colloid straining is relatively ineffective. In real, granular porous media, deviations from spherical shape, uniform grain size, and close packing will yield a range of ψ_c and S_c values over which pendular rings disconnect. The effect of ψ in this part of the model is analogous to that of a switch. At ψ greater than ψ_c (i.e., closer to zero) along the main wetting curve, film straining is ineffective, while $\psi \leq \psi_c$ enables film straining. We approximate the probability of pendular ring discontinuity by an integral normal probability function

$$F(\psi) = \frac{1}{p\sqrt{2\pi}}\int_0^{\psi} \exp\left[\frac{-(\psi - \psi_c)^2}{2p^2}\right] d\psi \qquad (2)$$

where $F(\psi)$ is the probability of pendular ring discontinuity, and p is the standard deviation of ψ over which pendular ring interconnections are broken. As $p \rightarrow 0$, the above function becomes a normalized step function. In the later modeling, values of ψ_c and p were set based on the median grain size and grain size ranges of the tested sands, respectively.

The above capillarity-based consideration provides estimates of when film straining can become important but does not account for the possibility of colloid transport in thin films. Capillary-based modeling of well-characterized porous media have been shown to underpredict saturation due to neglecting contributions from adsorbed films (*25*). Langmuir (*26*) derived expressions for thicknesses of water films, w, adsorbed on wettable vertical plates and on walls within capillaries (away from menisci). Various experimental tests of the Langmuir film thickness equation have shown qualitative agreement, although the model predictions below about 30 nm thickness begin to deviate significantly lower than measurements (*27*). Nevertheless, the model provides rough estimates of film thickness and its dependence on ψ. Following Langmuir's approach, we applied a simple modification to the original film equation for predicting the thickness of water films adsorbed on spherical grains (away from pendular ring regions), resulting in

$$w = \left(\frac{\epsilon\epsilon_o}{2}\right)^{1/2}\left(\frac{\pi kT}{ze}\right)\left(\frac{2\gamma}{R} - \psi\right)^{-1/2} \qquad (3A)$$

$$w = L\left(\frac{2\gamma}{R} - \psi\right)^{-1/2} \qquad (3B)$$

where ϵ is the dielectric constant of water, ϵ_o is the permittivity of free space, k is the Boltzmann constant, T is the Kelvin temperature, z is the ionic charge, and e is the electron charge. The constants associated with a given temperature and solution chemistry are grouped into the parameter L. Equations 3A and 3B differ from Langmuir's model for w along walls of a capillary above a static meniscus only through the interfacial curvature term, which is $-\gamma/R$ in the capillary case (as opposed to $2\gamma/R$). Predicted water film thicknesses of 1:1 electrolyte solutions at a temperature of 293 K are in the range of 20−40 nm at near-critical saturations for the three different size sands used.

While a hydrodynamic analysis of particle motion constrained within thin films is beyond the scope of this study, a tentative relation for describing particle straining in films is needed. We hypothesized that the drag force acting to transport colloids depends on both the average pore water velocity (v) and on w/d. We propose that film straining removes colloids from suspension at a rate approximately proportional to $v^{(1+h)}$, to $(d/w)^{\beta}$, and to C:

$$\frac{\partial C}{\partial t} \propto -Nv^{(1+h)}\left(\frac{d}{w}\right)^{\beta} C \qquad (4A)$$

or

$$\frac{\partial C}{\partial t} \propto -Nv^{(1+h)}\left[\frac{d}{L}\left(\frac{2\gamma}{R} - \psi\right)^{0.5}\right]^{\beta} C \qquad (4B)$$

where h, β, and N are empirical parameters to be determined. Flow velocity affects the colloid deposition rate in two different aspects expressed as two terms (1 and h) in the exponent of v. The v^1 term accounts for advection of colloids into the reference volume element. The v^h term empirically accounts for fluid drag on colloids, tending to keep them in motion and inhibiting deposition (with $h < 0$). This latter aspect of the velocity effect is consistent with conventional filtration theory. We lump the advection and drag effects together, simply for convenience in later comparisons between experiments and model predictions. Data from a study by Sharma et al. (*28*) on particle detachment from surfaces indicate that resistance to detachment is approximately related to v^h, with $h \approx -0.5$. This indicates that we may approximate the overall velocity effect on straining rate as proportional to $v^{0.5}$. However, it should be noted that Sharma et al. (*29*) did not include cases where $w < d$ and that it is quite possible that h is itself a function of w/d. Without further information, h was kept equal to −0.5.

Based on the preceding considerations, we can develop an approximate model that accounts for the local rate at which suspended colloids are strained by thin water films in unsaturated porous media. For a suspension of hydrophilic colloids (with $d \ll 0.05D$), film straining is not efficient unless $\psi \leq \psi_c = -B\gamma/R$. For $\psi \leq \psi_c$, film straining becomes important as w decreases relative to d, with the ψ dependence of w estimated from the Langmuir film equation. The local rate of film straining is due to the combined effects of capillary discontinuity of pendular rings, diminished mobilizing drag on colloids within thin films, and velocity influences. The local rate of colloid retardation during unsaturated flow is then approximated as

$$\left.\frac{\partial C}{\partial t}\right]_{\text{straining}} = -N\left\{\frac{1}{p\sqrt{2\pi}}\int_0^{\psi} \exp\left[\frac{-(\psi - \psi_c)^2}{2p^2}\right] d\psi\right\} \times \left[\frac{d}{L}\left(\frac{2\gamma}{R} - \psi\right)^{0.5}\right]^{\beta} v^{(1+h)} C \qquad (5A)$$

or

$$\left.\frac{\partial C}{\partial t}\right]_{\text{straining}} = -\mu C \qquad (5B)$$

where μ is constant for a system at constant characteristic grain and colloid sizes, solution chemistry, temperature, matric potential, and flow rate. Inclusion of v within μ is done for simplicity since individual experiments were run at constant v and for clearer application of the analytical solution to the colloid advection−dispersion equation described below. However, it will later be useful to compare straining efficiencies at a common amount of suspended colloid delivered. We define μ_o as the film-straining efficiency of a given system, obtained by factoring out the advection term. Thus μ_o is equal to μ/v. By setting $h = -0.5$ and $p = 100$ Pa for the coarse and medium sands, and $p = 700$ Pa for fine sand (calculated based on the grain size distribution of each sand), only N and β are adjustable parameters within μ_o. For geometrically similar porous media, one value of N and β

should adequately describe all possible combinations of saturation, grain size, and colloid size. The solution to the one-dimensional colloid advection−dispersion equation

$$\frac{\partial C}{\partial t} = D_h \frac{\partial^2 C}{\partial z^2} - v\frac{\partial C}{\partial z} - \mu C \tag{6}$$

with initial and boundary conditions

$$C(z,0) = 0 \tag{7A}$$

and

$$-D_h \frac{\partial C}{\partial z} + vC\Big|_{z=0} = vC_o \qquad (t > 0) \tag{7B}$$

is a special case of the more general solution given by van Genuchten (*29*). In eqs 6 and 7B, the dispersion coefficient is approximated by the hydrodynamic dispersion coefficient D_h, since the colloid diffusivities are much smaller than those for dissolved ions. The D_h values were estimated using a low dispersivity of 1 mm typical of short column systems, i.e., $D_h = (1\text{ mm})v$. Use of a low dispersivity is also more consistent with successful analyses of column filtration processes without inclusion of dispersion (*30*). C_o is the colloid concentration in the inflow solution. For the above initial and boundary conditions, without local colloid production, the solution to eq 6 is

$$\frac{C(z,t)}{C_o} = \frac{v}{v+u}\exp\left[\frac{(v-u)z}{2D_h}\right]\operatorname{erfc}\left[\frac{z-ut}{2\sqrt{D_h t}}\right] + \frac{v}{v-u}\exp\left[\frac{(v+u)z}{2D_h}\right]\operatorname{erfc}\left[\frac{z+ut}{2\sqrt{D_h t}}\right] + \frac{v^2}{2\mu D_h}\exp\left(\frac{vz}{D_h} - \mu t\right)\operatorname{erfc}\left[\frac{z+vt}{2\sqrt{D_h t}}\right] \tag{8}$$

where

$$u = v\sqrt{1 + \frac{4\mu D_h}{v^2}} \tag{9}$$

The local cumulative concentration of strained colloids is obtainable by substituting the solution of the advection−dispersion equation into eq 5 and integrating with respect to time. The total, suspended plus strained, colloid concentration at any location and time is then

$$\frac{C_\Sigma(z,t)}{C_o} = \frac{C(z,t)}{C_o} + \frac{\mu}{C_o}\int_0^t C(z,t')\,dt' \tag{10}$$

The effectiveness of the proposed model was tested through comparisons with column experiments in which characteristic grain and colloid sizes, matric potential, and flow rate were varied separately.

Experimental Methods and Materials

To test the film-straining model, a method of infiltrating colloid suspensions into packed sand columns was used. The primary concern in designing the experiments was to isolate the postulated film-straining mechanism, that is to minimize the possible effects of conventional straining, physical−chemical deposition, and attachment at gas−water interfaces. Well-rounded quartz sand was size-fractionated to specific ranges meeting the condition of $d/D \ll 0.05$. The reason for choosing quartz sand (Accusand, Unimin Co., New Canaan, CT) instead of soda-lime glass beads was to avoid the instability of surface chemical properties of grains (*31*). The sands were washed using an elaborate procedure (*17*) to remove all possibly attached organic and inorganic material. A very thorough cleaning process is essential in order to isolate the straining mechanism and to provide reproducibility in determination of colloid concentration with our method. Solution ionic strength was kept low (1.0 mM NaCl, pH 5.5) in all the experiments. Hydrophilic and negatively charged (carboxylate modified) polystyrene latex microspheres (Interfacial Dynamic Co., Portland, OR) were used as colloids. Three variables were tested: matric potential (and corresponding saturation), sand grain size (150−212, 212−425, and 425−500 μm), and colloid size (0.97, 0.28, 0.093, and 0.014 μm). The three pairs of matric potential−saturation curves were measured using a hanging column method (*20*). Sands for moisture characteristic determinations were packed to bulk densities of 1.75, 1.72, and 1.72 Mg m^{-3} (coarse, medium, and fine sands, respectively) and confined to a height of 15 mm in fritted glass filter funnels. The datum from which reservoir water levels were measured was taken at the mid-elevation of these sand packs, so that the uncertainty in matric head was <8 mm. The colloid transport columns were 0.34 m long and 19 mm i.d., assembled from 17 sections of 20 mm long acrylic tube. Columns were packed with clean dry sand to bulk densities mentioned previously and oriented vertically. The relatively small column i.d. was chosen based on the concern for matching our single injection source and minimizing possible fingering of flow. A uniform wetting front around the column wall was obvious in all the experiments. The particle concentrations at the inlet, C_o, were kept relatively low and varied from 107 to 1010 microspheres/mL for 0.97−0.014 μm size colloids, respectively. Each transport experiment was conducted by injecting a colloid suspension (at $C = C_o$) into the top of an initially dry column at a constant rate. This initial condition differs from that assumed in eqs 7 and 8, since saturation in the experiment varies locally, approximately as a step function with respect to time. However, upon passage of the sharp wetting front, essentially constant saturations are established. This suggests that the use of the analytical solution is justified within the wetted zone. The suitability of applying eqs 7 and 8 behind advancing wetting fronts was tested in a separate experiment. This experiment compared results based on two different initial conditions; initially air-dry and initially prewet to the steady-state saturation with colloid-free water. This test showed that the two initial conditions yielded essentially identical results, and infiltration of colloid suspensions into initially dry columns was selected for simplicity. Control of matric potential (and saturation) within a given column was obtained by applying water at a constant infiltration rate. A uniform saturation along a given column was achieved since the constant flux upper boundary condition produces unit gradient, gravity-driven flow in which the uniform unsaturated hydraulic conductivity equals the imposed flux density. Five different flow rates were tested, ranging from the Darcy velocity equal to the measured effectively saturated hydraulic conductivity (K_s) down to $10^{-4}K_s$, by reducing the rate 1 order of magnitude between each test. Injection was stopped when the wetting front reached the middle of the second to last section of the column. The column was laid down horizontally at the same time that the pump was turned off in order to terminate gravity-driven flow between sections. The column was then disassembled immediately. Water saturation was determined gravimetrically, and matric potential was obtained from predetermined main wetting characteristic curves of saturation vs matric potential. In order to determine colloid contents of individual column sections, 5 mL of deionized Nanopure water was added in the beaker containing the quantitatively recovered sand and mixed by shaking. Colloid concentrations of the diluted suspensions were then measured with spectrophotometer (Milton Roy Spectronic Model 601) with the wavelength varied from 430 to 220 nm for different size colloids. The sample from the last section was taken as a background reference (the infiltrating water

TABLE 1. Summary of Experimental Results

	Darcy velocity (m/s)	saturation (%)	matric potential (m)	water recovery (%)	colloid recovery (%)	μ_o[a] (1/m)
coarse sand	9.49E-04	96.2 ± 2.5	−0.05	97.0	99.9	0.00
425−500 μm	9.49E-05	61.1 ± 12.1	−0.13	96.5	102.3	0.27
K_{sat} = 9.49E-04 m/s	9.49E-06	29.1 ± 2.3	−0.18	96.7	101.4	2.96
n = 0.34	9.49E-07	24.6 ± 0.8	−0.20	96.7	99.9	8.84
colloids, 0.973 μm	9.49E-08	21.7 ± 3.3	−0.22	92.3	93.3	26.90
medium sand	4.75E-04	89.6 ± 2.4	−0.10	98.8 ± 0.8	99.6 ± 0.1	0.05
212−425 μm	4.75E-05	52.3 ± 4.1	−0.19	97.6 ± 0.4	101.8 ± 1.9	0.81
K_{sat} = 4.75E-04 m/s	4.75E-06	32.1 ± 2.3	−0.23	93.5 ± 2.3	99.4 ± 1.4	3.16
n = 0.34	4.75E-07	25.1 ± 0.7	−0.26	94.1 ± 1.3	98.3 ± 0.6	11.00
colloids, 0.973 μm	4.75E-08	20.5 ± 1.2	−0.28	88.8 ± 0.76	103.2 ± 8.4	35.00
fine sand	1.19E-04	88.9 ± 1.7	−0.18	98.0	98.3	0.01
150−212 μm	1.19E-05	52.4 ± 5.7	−0.37	96.8	106.3	2.73
K_{sat} = 1.19E-04 m/s	1.19E-06	34.4 ± 1.9	−0.43	95.4	107.1	10.60
n = 0.35	1.19E-07	26.2 ± 1.2	−0.48	94.5	103.7	33.60
colloids, 0.973 μm	1.19E-08	22.2 ± 1.3	−0.50	81.7	105.6	101.00

	colloid size (μm)	saturation (%)	matric potential (m)	water recovery (%)	colloid recovery (%)	μ_o[a] (1/m)
coarse sand	0.973	21.7 ± 3.3	−0.22	92.3	104.3	26.90
425−500 μm	0.282	21.7 ± 0.6	−0.22	89.2	99.3	11.80
Darcy velocity	0.093	20.1 ± 1.7	−0.23	92.0	90.0	6.02
9.49E-08 m/s	0.014	21.7 ± 0.5	−0.22	92.1	99.5	1.68
medium sand	0.973	20.5 ± 1.2	−0.28	88.8 ± 0.76	101.2 ± 8.4	35.00
212−425 μm	0.282	20.0 ± 0.6	−0.28	90.9	102.7	16.00
Darcy velocity	0.093	20.7 ± 0.4	−0.28	90.9	105.1	7.80
4.75E-08 m/s	0.014	20.7 ± 0.4	−0.28	91.7 ± 1.2	99.2 ± 3.7	2.17

[a] μ_o is the film-straining efficiency.

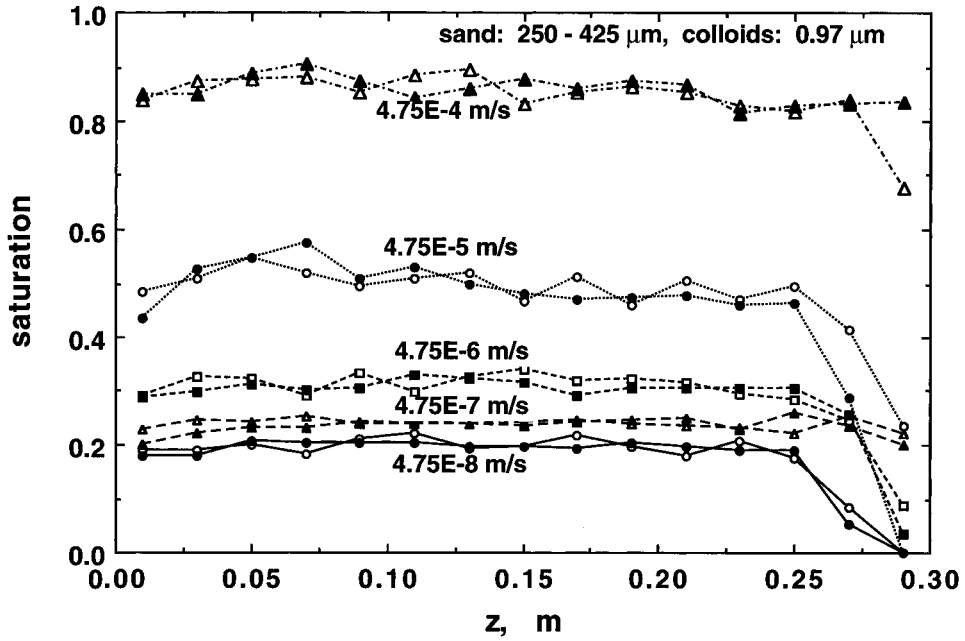

FIGURE 3. Examples of water saturation profiles along columns at the end of experiments. The last two data points in each of these profiles contains the wetting front and are not included in the reported average saturations.

did not reach this section). The total recovered colloid content from each segment was normalized to the volume of water in the segment and to the initial colloid concentration in the infiltrating water. Mass balances of water and colloids were calculated for each run.

Results and Discussion

The five flow rates applied to the three different grain-size sand columns, their corresponding saturation, matric head data [matric head = $\psi/(\rho g)$, ρ is the density of water, and g is the acceleration due to gravity], and the measured porosities and saturated hydraulic conductivity of the columns are listed in the first three sections of Table 1. The four colloid sizes used in two different sands, the applied Darcy velocities, saturations, and correspondent matric head of each column are listed in the last two sections of Table 1. The saturation value listed in Table 1 for each sand column is the average of its segment saturations (excluding the segment containing the wetting front). Data from medium-grain sands are averages of duplicate columns. Examples of saturation profiles within individual columns, including duplicate runs, are shown in Figure 3. Note that saturations were practically constant along a given column and that reproducibility between duplicate runs was excellent. The mass recovery data (in Table 1) also show good mass balances for both water and colloids. Evaporation compromised water mass balances in the slowest flow rate experiments. The matric potential values corresponding to the average column saturations were

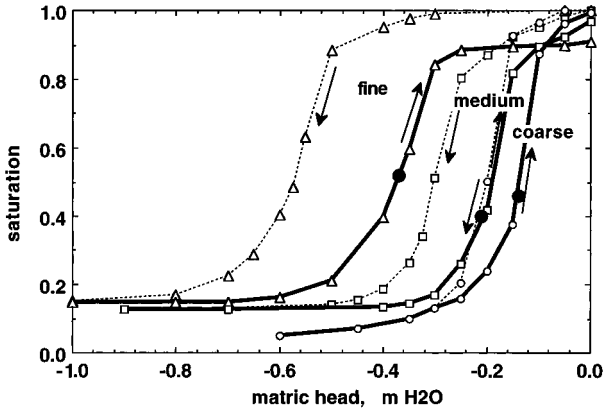

FIGURE 4. Measured water saturation versus matric head relations (main drainage and main wetting curves) for the three sands. The three solid cycles on the main wetting curves show model predicted critical matric head values of three sands and their corresponding saturations on the measured curves.

obtained from the main wetting branch of matric potential−saturation curves (Figure 4). The predicted ψ_c on the main wetting curve (based on median grain size and close packing) and the corresponding S_c are shown for each sand type in this figure. The close-pack model was selected for predicting ψ_c in our more random-packed sands because it better represents the critical condition. When ψ_c is achieved for wetting of close-pack microenvironments, pendular ring discontinuity is established in other more open-packed regions.

The experimental normalized colloid concentrations were obtained by normalizing the total recovered colloids (blank-subtracted spectrophotometer absorbance) from each column segment to the volume of water in the segment and to the initial concentration in the infiltrating water. The values of normalized absorbance from blanks were rather small and close to zero. The experimental results yielded profiles of total (mobile plus strained) colloids versus distance, which guided adjustment of the model parameters N and β. The best fits were obtained using N and β equal to 0.003 $(\text{m s})^{-1/2}$ and 0.65, respectively. The nonadjustable model input parameters were colloid and grain sizes, porosity, saturation, matric potential, and water velocity. The effect of saturation or matric potential on film straining was tested in three different sands (463 ± 38, 319 ± 107, and 181 ± 31 μm diameter sand grains) at five different saturations and using 1 μm colloids. The results are shown in Figure 5A−C along with modeled colloid concentration profiles (based on eq 10). Excellent agreement between the model and data was achieved. In Figure 5A−C, the 0.96, 0.90, and 0.89 saturation conditions resulted from infiltration at the near-saturated flow velocity (0.04−0.11 pore volume of air was trapped). The data showing essentially no colloid retardation indicate that neither conventional straining nor physical−chemical deposition were significant. In Figure 5A,B, data from the 0.61 and 0.52 saturations (both are above their critical saturations) also showing basically no retardation suggest that colloid attachment at the gas−water interfaces is insignificant under such unfavorable conditions. In each of these three sands, colloid retention only begins to become significant when saturation drops below the predicted critical values. Below S_c, colloid retardation efficiency increases rapidly with progressively lower saturations. Colloid transport becomes progressively retarded as thin films become dominant along flow pathways at lower S. At the lowest S in all three sands (0.21−0.22), more than 80% of the injected colloids (1.0 μm) are retained within 20% of the wetted length. The experiments conducted at different saturations were obtained under different flow rates, and as saturation and film thickness decrease, velocity decreases significantly (as shown in Table

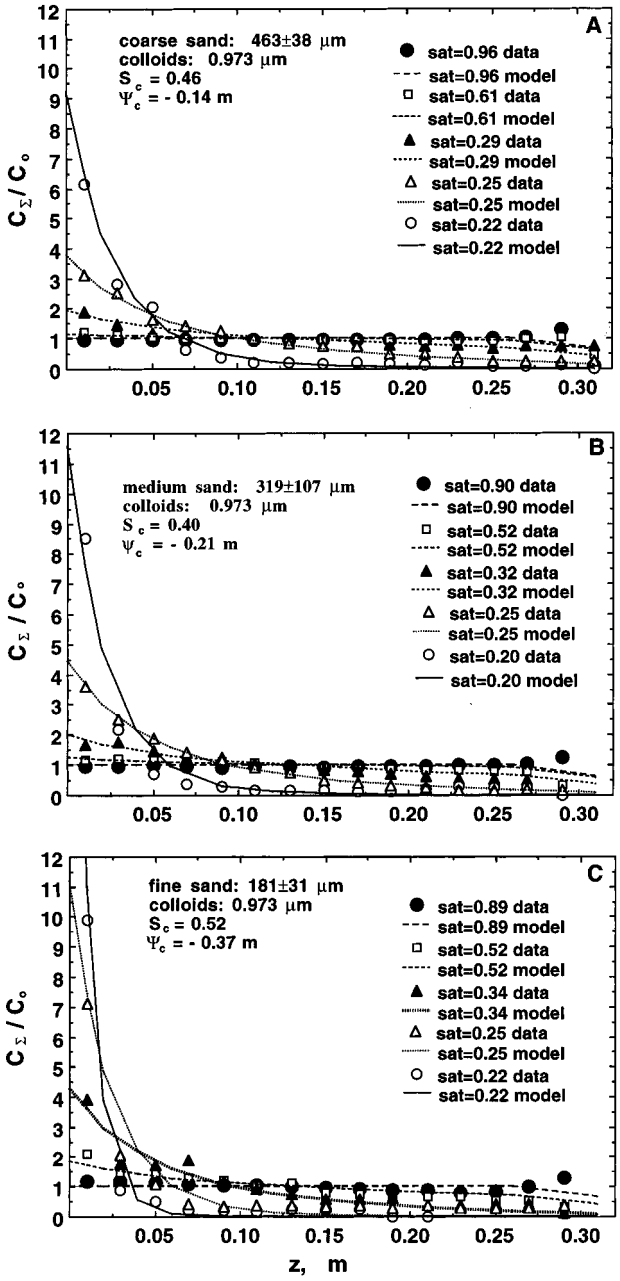

FIGURE 5. Saturation (matric potential) and grain size effects on total relative concentration profiles in (A) coarse, (B) medium, and (C) fine sand columns. Experimental data points are shown with film-straining model predictions.

1). Conventional filtration theory also predicts that deposition increases as velocity decreases mainly because sedimentation and diffusion become important under low flow rate. Sedimentation can play an important role under saturated conditions; however, we believe that sedimentation is not a major factor when the system is below its critical saturation. The film thicknesses below the critical saturations (30−40 nm) are thinner than the diameters of most of the colloids used in these experiments; therefore, there is no free room for significant sedimentation to occur (except within the pendular rings). Under these conditions, colloids are constrained to rolling along the grain surfaces, with the effect of flow velocity on colloid retention approximated by eq 4A. Thus, film straining is the only significant cause for colloid retardation in these experiments, as desired. The straining efficiency, μ_o, for each experimental condition is summarized in Table 1. These straining efficiencies were obtained using eq 5a, with the previously cited N and β values of 0.003 (m

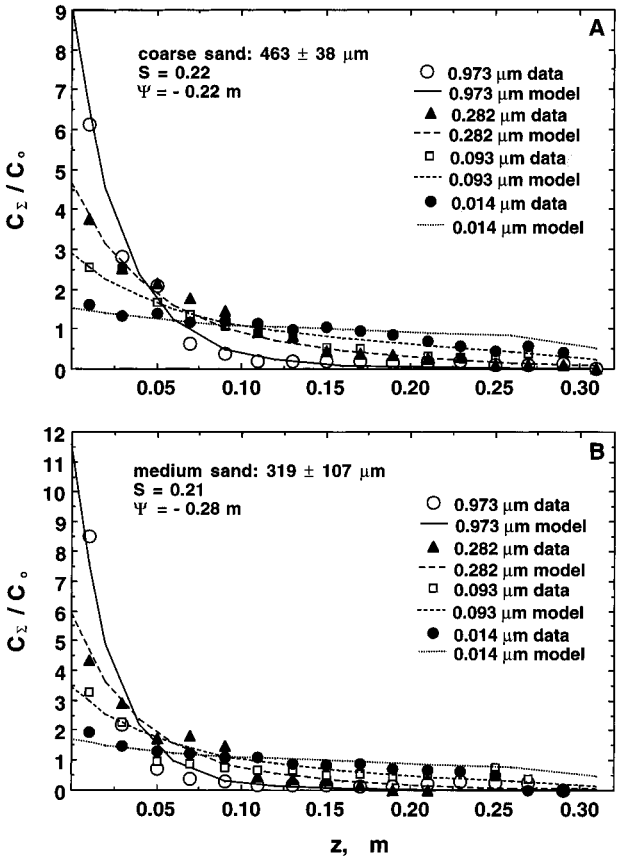

FIGURE 6. Colloid size effect on film straining in (A) coarse and (B) medium sand columns at saturations and matric potentials much lower than predicted critical values. Experimental results (data points) versus film-straininng model predictions.

s)$^{-1/2}$ and 0.65, respectively. Note that μ_o is very small for high values of S and ψ and increases significantly for values lower than S_c and ψ_c. Also note that the last two relative colloid concentration data points near the end of each high saturation column are consistently greater than 1 for all three grain sizes. We believe this feature is caused by size exclusion, a phenomenon that was not included in our model.

The effect of grain size on film straining can also be inferred by comparison of data from the three different sands. At a common value of saturation in Figure 5A–C, film-straining efficiency is higher in finer sand than in coarser sand. Note that the increased retardation in finer sand is not caused by conventional straining, but by thinner water films on finer grain surfaces at a common saturation. Recall (eq 1 and also Figure 4) that for the nearly geometrically similar porous media investigated, the magnitude of ψ scales inversely with respect to grain size at a common value of saturation. Also recall from eq 3 that for a common value of matric potential the adsorbed films are thinner on finer grain surfaces than on coarser grain surfaces. Therefore at a common value of saturation, finer-grained media with thinner water films permit more efficient film straining than coarse-grained media.

The film-straining mechanism was further tested by using four different size colloids in the coarse and medium sand columns at saturations much lower than the critical saturation. Comparisons between data and corresponding model results are shown in Figure 6A,B, with good agreement obtained for all the cases. In each panel, colloid size was the only variable, and the colloids moved through the columns with the same saturation under the same flow rate. Figure 6A,B shows decreasing deposition as size decreases from 1 to 0.014 μm in both coarse and medium sands. This outcome is opposite that predicted based on Brownian deposition in conventional filtration theory for saturated porous media and can only be explained by the film-straining theory. The results show that the film-straining efficiency is proportional to colloid size. Film thicknesses in these experiments are in the range of 0.020–0.040 μm, based on eq 3, thus the ratio of colloid size to film thickness must be a key factor for film straining. Note that only the finest colloids, 0.014 μm, moved through these columns relatively freely and that these were the only particles smaller than the predicted film thickness (20–40 nm). Recalling our conceptual model (Figure 2), the condition of the finest sized colloids are depicted in Figure 2A and that of the three larger sized colloids are depicted in Figure 2B.

Excellent agreement with experiments (covering a wide range of conditions) supports the conceptual basis of this model. Systems must be above certain critical saturation values in order for colloid transport to be significant. For a given saturation, colloid transport is more efficient in a porous medium with larger size grains than that with smaller grains due to related differences in water film thickness. For the colloids smaller than the thickness of adsorbed thin water films, even when the system matric potential and saturation are much lower than their critical values, colloids can still be transported efficiently. Therefore, effective penetration of colloids through the vadose zone occurs under conditions of $S > S_c$, ($\psi > \psi_c$), and $d/w < 1$. Temporal variations in soil profile saturation and infiltration rate result in strongly nonlinear colloid mobility in the vicinity of S_c. The strong saturation dependence of film-straining efficiency, μ_o, implies efficient mobilization of colloids during high-intensity rainfall events. Additional factors influencing film straining in more general cases include distributions in grain size, grain shape and surface roughness, grain packing and aggregation, and colloid shape. Additional research will be needed to examine more complex systems. While the focus of this study was on film straining, all other established colloid retardation mechanisms in both saturated and unsaturated porous media (physical–chemical deposition, conventional straining, and attachment onto gas–water interfaces) can be directly superimposed on this model.

Acknowledgments

This work was carried out under U.S. Department of Energy Contract DE-AC03-76SF-00098. Funding was provided by the Laboratory Directed Research and Development program of Lawrence Berkeley National Laboratory and the U.S. Department of Energy, Basic Energy Sciences, Geosciences Research Program. We thank the anonymous reviewers for helpful comments.

Literature Cited

(1) McDowell-Boyer, L. M.; Hunt, J. R.; Sitar, N. *Water Resour. Res.* **1986**, *22*, 1901–1921.
(2) McCarthy, J. F.; Zachara, J. M. *Environ. Sci. Technol.* **1989**, *23*, 496–502.
(3) Yao, K. M.; Habibian, M. T.; O'Melia, C. R. *Environ. Sci. Technol.* **1971**, *5*, 1105–1112.
(4) Rajagopalan, R.; Tien, C. *J. Am. Inst. Chem. Eng.* **1976**, *22*, 523–533.
(5) Tien, C.; Payatakes, A. C. *AIChE J.* **1979**, *25*, 737–759.
(6) Herzig, J. P.; Leclerc, D. M.; Le Goff, P. *Ind. Eng. Chem.* **1970**, *62*, 156–157.
(7) Sheppard, J. C.; Campbell, M. J.; Cheng, T.; Kittrick, J. A. *Environ. Sci Technol.* **1980**, *14*, 1349–1353.
(8) Buddemeier, R. W.; Hunt, J. R. *Appl. Geochem.* **1988**, *3*, 535–548.
(9) Harvey, R. W.; George, L. H.; Smith, R. L.; LeBlanc, D. R. *Environ. Sci. Technol.* **1989**, *23*, 51–56.
(10) Penrose, W. R.; Polzed, W. L.; Essington, E. H.; Nelson, D. M.; Orlandini, K. A. *Environ. Sci. Technol.* **1990**, *24*, 228–234.
(11) Elimelech, M., O'Melia, C. R. *Langmuir* **1991**, *6*, 1153–1163.
(12) Ryan, J. N.; Gschwend, P. M. *Water Resour. Res.* **1990**, *26*, 307–317.
(13) Lance, J. C.; Gerba, C. P. *Appl. Environ. Microbiol.* **1984**, *47*, 335–337.
(14) Huysman, F.; Verstraete, W. *Soil Biol. Biochem.* **1993**, *25*, 91–97.

(15) Powelson, D. K.; Simpson, J. R.; Gerba, P. J. *Environ. Qual.* **1990**, *19*, 396−401.
(16) Wan, J.; Wilson, J. L. *Water Resour. Res.* **1994**, *30*, 11−23.
(17) Wan, J.; Wilson, J. L. *Water Resour. Res.* **1994**, *30*, 857−864.
(18) Wan, J.; Wilson, J. L.; Kieft, T. L. *Appl. Environ. Microbiol.* **1994**, *60*, 509−516.
(19) Corapcioglu, Y. M.; Choi, H. *Water Resour. Res.* **1996**, *32*, 3437−3449.
(20) Hillel, D. *Fundamentals of Soil Physics*; Academic Press: New York, 1980.
(21) Sposito, G. *The Thermodynamics of Soil Solutions*; Oxford University Press: Oxford, 1981.
(22) Miller, E. E.; Miller, R. D. *J. Appl. Phys.* **1956**, *27*, 324−332.
(23) Fisher, R. A. *J. Agric. Sci.* **1926**, *16*, 492−505.
(24) Melrose, J. C.; Wallick, G. C. *J. Phys. Chem.* **1967**, *71*, 3676−3678.
(25) Waldron, L. J.; McMurdie, J. L.; Vomocil, J. A. *Soil Sci. Soc. Am. Proc.* **1961**, *25*, 265−267.
(26) Langmuir, I. *Science (Washington, DC)* **1938**, *88*, 430−432.
(27) Israelachvili, J. N. *Intermolecular and Surface Forces*, 2nd ed.; Academic Press: San Diego, 1992.
(28) Sharma, M. M.; Chamoun, H.; Sita Rama Sarma, D. S. H.; Schechter, R. S. *J. Colloid Interface Sci.* **1992**, *149*, 121−134.
(29) van Genuchten, M. Th. J. *Hydrol.* **1981**, *49*, 213−233.
(30) Tien, C. *Granular Filtration of Aerosols and Hydrosols*; Butterworths Publishers: Boston, 1989.
(31) Litton, G. M.; Olson, T. M. *Environ. Sci. Technol.* **1993**, *27*, 185−193.

Received for review January 8, 1997. Revised manuscript received April 14, 1997. Accepted April 16, 1997.[⊗]

ES970017Q

[⊗] Abstract published in *Advance ACS Abstracts,* June 15, 1997.